Available online at www.sciencedirect.com
ScienceDirect
International Journal of Heat and Mass Transfer 51 (2008) 4651–4658
International Journal of HEAT and MASS TRANSFER
www.elsevier.com/locate/ijhmt

Axial heat conduction in a moving semi-infinite fluid

A. Haji-Sheikh [a,*], Donald E. Amos [b,1], J.V. Beck [c]

[a] Department of Mechanical and Aerospace Engineering, The University of Texas at Arlington, Arlington, TX 76019-0023, USA
[b] Sandia National Laboratories, Albuquerque, NM 87185, USA
[c] Department of Mechanical Engineering Michigan State University, East Lansing, MI 48824-1226, USA

Received 27 November 2007; received in revised form 26 January 2008
Available online 11 April 2008

Abstract

This paper considers the steady state conduction of heat from a wall to a fluid moving at a uniform velocity. The wall is heated by a step change in temperature. Although this appears to be a classical heat conduction problem, its application to various convective heat transfer problems is new. The mathematical procedure leads to the computation of the temperature field and the heat transfer coefficient. In the presence of a step change in the wall temperature, it is shown that the Stanton number is a function of the Peclet number alone. The acquired analytical results show that, near the thermal entrance location, heat conduction dominates and the local heat flux becomes independent of velocity. This phenomenon applies to classical convection problems in various-shaped ducts.

Keywords: Heat transfer; Moving boundary; Axial conduction; Slug flow; Thermal entrance

1. Introduction

Conduction of heat in the presence of a moving wall is widely available in the literature [1,2]. The emphasis of this paper is to determine the effect of axial conduction of heat, in the flow direction parallel to a wall. Also, the fluid can be viewed as a stationary semi-infinite domain with a moving wall temperature at $\hat{y} = 0$. A simple model, as shown in Fig. 1, is selected to show this effect and it describes a fluid flowing at a uniform velocity over an infinite plate whose temperature is T_i when $\hat{x} < 0$ and suddenly changes to T_w when $\hat{x} > 0$. This mathematical model provides useful information as to the behavior of the heat transfer near the thermal entrance location within the flow in ducts.

Knowledge of heat flux near the location where heating begins has application to convective heat transfer in ducts when the axial conduction effect is significant. This phenomenon has been studied in the past for free flow through ducts using various numerical schemes [3–7] and a complete extended Graetz solution is in [8]. The contribution of axial thermal conduction in porous passages, with walls at uniform temperature, are numerically determined and reported in [9] for parallel plate channel and in [10] for circular ducts. Also, it has applications in micro-devices [11] and cooling of electronic systems, especially when the ducts are filled with fluid saturated porous materials [12,13]. Accordingly, the flow in channels filled with fluid saturated hyperporous metallic foam [14] is of interest for cooling of electronic devices. Experimental data in [15] show that the Peclet number in channels filled with fluid saturated porous aluminum foam can become relatively small and, under this condition, the contribution of axial conduction becomes significant.

Lahjomri and Oubarra present a procedure in [8] for determination of heat transfer in the presence of axial conduction to free flow through parallel plate channels and circular ducts using a modified Graetz solution method. Also, a study of the effect of axial thermal conduction to the heat transfer phenomena in these ducts, filled with fluid saturated porous materials, is in Minkowycz and Haji-Sheikh [16].

* Corresponding author. Tel.: +1 817 272 2010; fax: +1 817 272 2603.
E-mail address: haji@uta.edu (A. Haji-Sheikh).
[1] Retired.

0017-9310/$ - see front matter © 2008 Elsevier Ltd. All rights reserved.
doi:10.1016/j.ijheatmasstransfer.2008.01.025

Nomenclature

c_p	specific heat, J/kg K	W	fluid layer thickness, m
E	energy, W	x	$\hat{x}/L_c$
h	heat transfer coefficient, W/m^2 K	$\hat{x}$	axial coordinate, m
k	thermal conductivity, W/m K	y	$\hat{y}/L_c$
L_c	characteristic length	$\hat{y},\hat{z}$	coordinates, m
Nu_x	$h\hat{x}/k$		
Pe	Peclet number, UL_c/α	*Greek symbols*	
Pe_x	Peclet number, $U\hat{x}/\alpha$	α	thermal diffusivity, m^2/s
q_w	wall heat flux, W/m^2	β	dummy variable
$Q_{1,2}$	wall heat flux between $\hat{x}_1$ and $\hat{x}_2$, W/m	ζ	$U\hat{x}/(2\alpha)$
Q^*	dimensionless total wall heat flux	λ	dummy variable
St	Stanton number, $h/(\rho c_p U)$	θ	dimensionless temperature
T_i	wall temperature when $\hat{x}<0$, K	ρ	density, kg/m^3
T_w	wall temperature when $\hat{x}>0$, K	Ψ	special function
U	velocity, m/s	ω	$Pe/2$

The case of slug flow appears in fluid flow through porous passages when the permeability is small. The studies reported here show that, for other cases, this slug flow assumption provides an asymptotic value for heat transfer near the location where the wall temperature changes. The following mathematical formulations show that both slug flow and no flow conditions approach the same values in the vicinity of thermal entrances location. This implies that near the thermal entrance location the velocity effect becomes negligibly small.

2. Mathematical formulation

For study of heat transfer at very small x values, a non-series solution is desirable. Alternatively, two limiting solutions are sought: one assumes no flow condition as a lower limit and the other assumes a slug flow as the upper limit. The actual solution is expected to fall between these two solutions. The subsequent formulation considers flow in a semi-infinite region, shown in Fig. 1, whose solution provides these limiting cases. The steady state energy equation assuming constant thermophysical properties, is

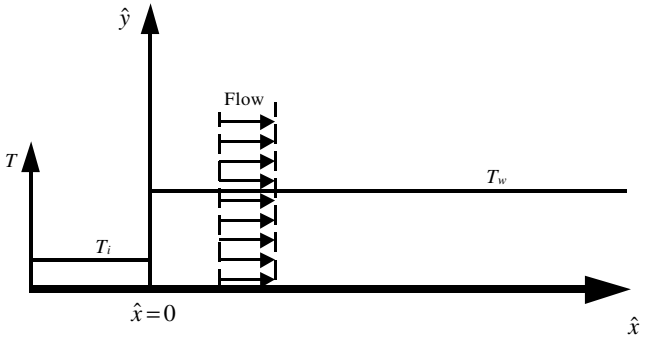

Fig. 1. Schematic of a semi-infinite region with temperature change at $\hat{x}=0$.

$$k\left(\frac{\partial^2 T}{\partial \hat{x}^2}+\frac{\partial^2 T}{\partial \hat{y}^2}\right)=\rho c_p U\frac{\partial T}{\partial \hat{x}} \tag{1}$$

When the dimensionless temperature is defined as $\theta=(T-T_i)/(T_w-T_i)$, Eq. (1) takes the form

$$\frac{\partial^2\theta}{\partial x^2}+\frac{\partial^2\theta}{\partial y^2}=Pe\frac{\partial\theta}{\partial x} \tag{2}$$

where $x=\hat{x}/L_c$, $y=\hat{y}/L_c$, $Pe=UL_c/\alpha$, and U is the velocity. The parameter L_c is an arbitrarily selected quantity equal to the width of the fluid layer $W=1$ m in the $\hat{z}$ direction perpendicular to $\hat{x}\hat{y}$-plane as depicted in Fig. 1. It is also possible to select $L_c=\alpha/U$; however, in the preliminary formulation $L_c=1$ m and this makes $x=\hat{x}$, $y=\hat{y}$. The boundary conditions for inclusion with Eq. (2) are

$$\begin{cases}\theta(x,\infty)=0\\ \theta(x,0)=0, \quad \text{when } x<0 \quad \text{and} \quad \theta(x,0)=1, \quad \text{when } x>0\\ \theta(\pm\infty,y)=\text{finite}\end{cases} \tag{3}$$

Additionally, a special solution assuming no flow, when $Pe=0$, satisfies the following relation:

$$\frac{\partial^2\theta}{\partial x^2}+\frac{\partial^2\theta}{\partial y^2}=0 \tag{4}$$

subject to the same boundary conditions as given by Eq. (3). The solution of Eq. (4) in a semi-infinite plane is elementary; it becomes a one-dimensional problem in cylindrical coordinates whose solution is

$$\theta=1-\frac{\phi}{\pi} \tag{5a}$$

where ϕ is the angular coordinate. Since $\tan\phi = y/x$ when $x > 0$ and $\tan(\pi - \phi) = y/|x|$ when $x < 0$, Eq. (5a) takes the form

$$\theta = \begin{cases} 1 - \frac{1}{\pi}\tan^{-1}\left(\frac{y}{x}\right) & \text{when } x > 0 \\ \frac{1}{\pi}\tan^{-1}\left(\frac{y}{|x|}\right) & \text{when } x < 0 \end{cases} \tag{5b}$$

Now, return to the solution of Eq. (2) which is the primary emphasis of this paper. For convenience of the algebra, the transformation

$$\theta(x,y) = \mathrm{e}^{\omega x}\psi(x,y) \tag{6}$$

reduces Eq. (2) to

$$\frac{\partial^2\psi}{\partial x^2} + \frac{\partial^2\psi}{\partial y^2} - \omega^2\psi = 0 \tag{7}$$

where $\omega = Pe/2$. Solution of this equation is obtainable using the standard separation of variables technique by letting $\psi = X(x)Y(y)$ to obtain

$$\frac{X''}{X} = -\frac{Y''}{Y} + \omega^2 = -\lambda^2 \tag{8}$$

with λ being a constant. Eq. (8) represents two ordinary differential equations whose solutions are $X = \exp(\pm \mathrm{i}\lambda x)$ and $Y = \exp\left(-y\sqrt{\lambda^2+\omega^2}\right)$. The application of an integral transform, in [17] and in [18, Section 17.21, P. 1183], to the $X(x)Y(y)$ product gives the value of ψ; that is

$$\psi(x,y) = \int_{-\infty}^{+\infty} A(\lambda)\exp(\mathrm{i}\lambda x)\exp\left(-y\sqrt{\lambda^2+\omega^2}\right)\mathrm{d}\lambda \tag{9}$$

and then Eq. (6) provides the solution for Eq. (2),

$$\theta(x,y) = \mathrm{e}^{\omega x}\int_{-\infty}^{+\infty} A(\lambda)\exp(\mathrm{i}\lambda x)\exp\left(-y\sqrt{\lambda^2+\omega^2}\right)\mathrm{d}\lambda \tag{10}$$

The condition at the wall $\theta(x,0) = f(x)$ in conjunction with Eq. (6) makes

$$A(\lambda) = \frac{1}{2\pi}\int_{-\infty}^{+\infty}[\exp(-\omega\xi)f(\xi)]\exp(-\mathrm{i}\lambda\xi)\,\mathrm{d}\xi \tag{11}$$

When the function $f(x)$ is defined as

$$f(x) = \begin{cases} 0 & \text{when } x < 0 \\ 1 & \text{when } x > 0 \end{cases} \tag{12}$$

Eq. (11) become

$$A(\lambda) = \frac{1}{2\pi}\int_0^{+\infty}\exp[-(\omega+\mathrm{i}\lambda)\xi]\,\mathrm{d}\xi = \frac{1}{2\pi}\left(\frac{1}{\omega+\mathrm{i}\lambda}\right) \tag{13}$$

Following the substitution for $A(\lambda)$, Eq. (10) takes the following form:

$$\theta(x,y) = \frac{\mathrm{e}^{\omega x}}{2\pi}\left[\int_{-\infty}^{0}\frac{\mathrm{e}^{\mathrm{i}\lambda x}\mathrm{e}^{-y\sqrt{\lambda^2+\omega^2}}}{\omega+\mathrm{i}\lambda}\,\mathrm{d}\lambda + \int_0^{\infty}\frac{\mathrm{e}^{\mathrm{i}\lambda x}\mathrm{e}^{-y\sqrt{\lambda^2+\omega^2}}}{\omega+\mathrm{i}\lambda}\right]\mathrm{d}\lambda \tag{14}$$

This equation provides the solution for a positive x and for a negative x. The solution presented by Eq. (14) has real and imaginary components. This equation is reduced by multiplying the numerators and the denominators by $\omega - \mathrm{i}\lambda$, replacing $\exp(i\lambda x)$ by $\cos(\lambda x) + \mathrm{i}\sin(\lambda x)$, retaining the real parts, and following standard algebraic steps. Then, the complex integrals within Eq. (14) yield the temperature solution as

$$\theta(x,y) = \frac{\mathrm{e}^{-\omega|x|}}{\pi}\left[\int_0^{+\infty}\omega\mathrm{e}^{-y\sqrt{\lambda^2+\omega^2}}\frac{\cos(\lambda\,|\,x\,|)}{\lambda^2+\omega^2}\,\mathrm{d}\lambda - \int_0^{+\infty}\mathrm{e}^{-y\sqrt{\lambda^2+\omega^2}}\frac{\lambda\sin(\lambda\,|\,x\,|)}{\lambda^2+\omega^2}\,\mathrm{d}\lambda\right] \tag{15a}$$

when $x < 0$ and

$$\theta(x,y) = \frac{\mathrm{e}^{\omega x}}{\pi}\left[\int_0^{+\infty}\omega\mathrm{e}^{-y\sqrt{\lambda^2+\omega^2}}\frac{\cos(\lambda x)}{\lambda^2+\omega^2}\,\mathrm{d}\lambda + \int_0^{+\infty}\mathrm{e}^{-y\sqrt{\lambda^2+\omega^2}}\frac{\lambda\sin(\lambda x)}{\lambda^2+\omega^2}\,\mathrm{d}\lambda\right] \tag{15b}$$

when $x > 0$. For the purpose of verification, one can show that Eqs. (15a) and (15b) when $\omega = 0$ reduce to

$$\begin{aligned}\theta(x,y) &= \frac{1}{\pi}\left[\int_0^{\infty}\frac{1}{\beta^2+1}\mathrm{d}\beta \pm \int_0^{\infty}\mathrm{e}^{-y\lambda}\frac{\sin(\lambda\,|\,x\,|)}{\lambda}\,\mathrm{d}\lambda\right] \\ &= \frac{1}{2} \pm \frac{1}{\pi}\tan^{-1}\left(\frac{|\,x\,|}{y}\right) \\ &= \begin{cases} 1 - \frac{1}{\pi}\tan^{-1}\left(\frac{y}{x}\right), & x > 0 \\ \frac{1}{\pi}\tan^{-1}\left(\frac{y}{|x|}\right), & x < 0 \end{cases}\end{aligned} \tag{16}$$

Eqs. (15a) and (15b) do not have good convergence characteristics; therefore, alternative forms with better convergence behaviors are sought. Examination of Eq. (3.961) in [18] shows two possible useful relations to improve the convergence, they are

$$\int_0^{+\infty}\mathrm{e}^{-y\sqrt{\lambda^2+\omega^2}}\frac{\lambda\sin(\lambda x)}{\sqrt{\lambda^2+\omega^2}}\,\mathrm{d}\lambda = \frac{\omega x}{\sqrt{x^2+y^2}}K_1\left[\omega\sqrt{x^2+y^2}\right] \tag{17a}$$

and

$$\int_0^{+\infty}\mathrm{e}^{-y\sqrt{\lambda^2+\omega^2}}\frac{\cos(\lambda x)}{\sqrt{\lambda^2+\omega^2}}\,\mathrm{d}\lambda = K_0\left[\omega\sqrt{x^2+y^2}\right] \tag{17b}$$

where K_0 and K_1 are the modified Bessel functions. Once Eq. (15a) or Eq. (15b) is differentiated with respect to y, the terms on the right side contain the integrals appearing on the left side of Eqs. (17a) and (17b). After differentiation of Eqs. (15a) and (15b) with respect to y and subsequent substitutions using Eqs. (17a) and (17b), the results are

$$\frac{\partial\theta(x,y)}{\partial y} = -\frac{\mathrm{e}^{-\omega|x|}}{\pi}\left\{\omega K_0\left[\omega\sqrt{x^2+y^2}\right] - \frac{\omega\,|\,x\,|}{\sqrt{z^2+y^2}}K_1\left[\omega\sqrt{x^2+y^2}\right]\right\} \tag{18a}$$

for $x<0$ and

$$\frac{\partial\theta(x,y)}{\partial y}=-\frac{e^{\omega x}}{\pi}\left\{\omega K_0\left[\omega\sqrt{x^2+y^2}\right]+\frac{\omega x}{\sqrt{x^2+y^2}}K_1\left[\omega\sqrt{x^2+y^2}\right]\right\} \tag{18b}$$

for $x>0$. Next, the integration of Eqs. (18a) and (18b) over y yields the final solutions

$$\theta(x,y)=-\frac{e^{-\omega|x|}}{\pi}\left[\omega\int_0^y K_0(\omega\sqrt{x^2+\eta^2})\,d\eta-\omega\,|\,x\,|\int_0^y\frac{K_1(\omega\sqrt{x^2+\eta^2})}{\sqrt{x^2+\eta^2}}\,d\eta\right] \tag{19a}$$

when $x<0$ and

$$\theta(x,y)=1-\frac{e^{\omega x}}{\pi}\left[\omega\int_0^y K_0(\omega\sqrt{x^2+\eta^2})\,d\eta+\omega x\int_0^y\frac{K_1(\omega\sqrt{x^2+\eta^2})}{\sqrt{x^2+\eta^2}}\,d\eta\right] \tag{19b}$$

when $x>0$. These are convenient solution forms since their y-derivatives at the wall are

$$\left.\frac{\partial\theta(x,y)}{\partial y}\right|_{y=0}=-\frac{\omega e^{-\omega|x|}}{\pi}[K_0(\omega\,|\,x\,|)-K_1(\omega\,|\,x\,|)]\quad\text{when } x<0 \tag{20a}$$

and

$$\left.\frac{\partial\theta(x,y)}{\partial y}\right|_{y=0}=-\frac{\omega e^{\omega x}}{\pi}[K_0(\omega x)+K_1(\omega x)]\quad\text{when } x>0 \tag{20b}$$

If the magnitude of x is sufficiently small, Eq. (9.6.13) in [19] can be used to get an approximation for the $K_0(z)$ Bessel function as

$$K_0(z)\ \cong\ -[\ln(z/2)+0.5772](1+z^2/2) \tag{21a}$$

and, from Eq. (9.6.11) in [19], an approximation for the $K_1(z)$ Bessel function is

$$K_1(z)\ \cong\ \frac{1}{z}+\frac{z}{2}\ln(z/2) \tag{21b}$$

Eqs. (21a) and (21b) can produce the values for these Bessel functions with four or more accurate significant figures when $z\leqslant 0.025$.

3. Determination of local wall heat flux

Using the heat flux definition, $q_w=-k\partial T/\partial y|_{y=0}$, it is observed that Eqs. (20a) and (20b) are related to the wall heat flux. These quantities are used to determine expressions for the wall heat flux and then to get the local heat transfer coefficient $h=q_w/(T_w-T_i)$; then, the local Stanton number, $St=h/(\rho c_p U)$, becomes

$$St=\frac{q_w}{k(T_w-T_i)}\frac{\alpha}{U}=-\frac{1}{2\omega}\left.\frac{\partial\theta(x,y)}{\partial y}\right|_{y=0} \tag{22}$$

Following standard substitutions, using Eqs. (20a) and (20b), the Stanton number is

$$St=\frac{e^{-|Pe_x|/2}}{2\pi}[K_0(|\,Pe_x\,|/2)-K_1(|\,Pe_x\,|/2)]\quad\text{when } x<0 \tag{23a}$$

and

$$St=\frac{e^{Pe_x/2}}{2\pi}[K_0(Pe_x/2)+K_1(Pe_x/2)]\quad\text{when } x>0 \tag{23b}$$

where $Pe_x=U\hat{x}/\alpha$ and $|\,Pe_x\,|=U\,|\,\hat{x}\,|/\alpha$ since $\omega=U/\alpha$.

4. Total wall heat flux

The total heat flux is needed for the design of cooling devices when the wall is heated discretely. The heat flux leaving a differential element $W\times dx$ in the $\hat{x}\hat{z}$-plane with $W=1$ m is $dQ\times 1=h(T_w-T_i)\times 1\times d\hat{x}$. Then, the heat flux per unit length in z-direction is obtainable by integration of dQ over $\hat{x}$,

$$Q_{1,2}=\int_{\hat{x}_1}^{\hat{x}_2}h(T_w-T_i)\,d\hat{x} \tag{24a}$$

In dimensionless space, when $\zeta=Pe_x/2$, Eq. (24a) becomes

$$\frac{Q_{1,2}}{k(T_w-T_i)}=\frac{2\alpha}{kU}\int_{\zeta_1}^{\zeta_2}h\,d\zeta=2\int_{\zeta_1}^{\zeta_2}St\,d\zeta \tag{24b}$$

This definition of total heat flow in conjunction with Eqs. (23a) and (23b) yields the relations,

$$\frac{Q_{1,2}}{k(T_w-T_i)}=\frac{1}{\pi}\int_{\zeta_1}^{\zeta_2}e^{-|\zeta|}[K_0(|\,\zeta\,|)-K_1(|\,\zeta\,|)]\,d\zeta\quad\text{when } \zeta<0 \tag{25a}$$

or

$$\frac{Q_{1,2}}{k(T_w-T_i)}=\frac{1}{\pi}\int_{\zeta_1}^{\zeta_2}e^{\zeta}[K_0(\zeta)+K_1(\zeta)]\,d\zeta\quad\text{when } \zeta>0 \tag{25b}$$

Since $Q_{1,2}$ has the dimension of W/m, then, the quantity $Q_{1,2}/[k(T_w-T_i)]$ represents the dimensionless total wall heat flux between ζ_1 and ζ_2.

The next task is the determination of these integrals. The analysis begins by using Eq. (11.3.15) in [19] (with $\nu=0$) to get

$$\int_0^{\zeta}e^{-\zeta}K_0(\zeta)\,d\zeta=\zeta e^{-\zeta}[K_0(\zeta)-K_1(\zeta)]+1 \tag{26a}$$

$$\int_0^{\zeta}e^{\zeta}K_0(\zeta)\,d\zeta=\zeta e^{\zeta}[K_0(\zeta)+K_1(\zeta)]-1 \tag{26b}$$

After differentiating the variables on the left side of following equations

$$d[e^{-\zeta}K_0(\zeta)] = -e^{-\zeta}K_0(\zeta)\,d\zeta - e^{-\zeta}K_1(\zeta)\,d\zeta \quad (27a)$$

$$d[e^{\zeta}K_0(\zeta)] = e^{\zeta}K_0(\zeta)\,d\zeta - e^{\zeta}K_1(\zeta)\,d\zeta \quad (27b)$$

and subsequent integrating of both sides, one gets other needed integrals

$$\int e^{-\zeta}K_1(\zeta)\,d\zeta = -\int e^{-\zeta}K_0(\zeta)\,d\zeta - e^{-\zeta}K_0(\zeta) \quad (28a)$$

$$\int e^{\zeta}K_1(\zeta)\,d\zeta = \int e^{\zeta}K_0(\zeta)\,d\zeta - e^{\zeta}K_0(\zeta) \quad (28b)$$

and then, using Eqs. (26a) and (26b), they become

$$\int e^{-\zeta}K_1(\zeta)\,d\zeta = -\zeta e^{-\zeta}[K_0(\zeta) - K_1(\zeta)] - e^{-\zeta}K_0(\zeta) \quad (29a)$$

$$\int e^{\zeta}K_1(\zeta)\,d\zeta = \zeta e^{\zeta}[K_0(\zeta) + K_1(\zeta)] - e^{\zeta}K_0(\zeta) \quad (29b)$$

Now, the mathematical relations presented in Eqs. (25a), (25b), (29a),(29b) are used for the determination of $Q^* = Q/[k(T_w - T_i)]$ as related to the total wall heat flux. Following appropriate substitutions, the indefinite integrals for Q^* are

$$Q^* = \frac{1}{\pi}\int e^{-|\zeta|}[K_0(|\zeta|) - K_1(|\zeta|)]\,d\zeta \quad \text{when } \zeta < 0 \quad (30a)$$

$$Q^* = \frac{1}{\pi}\int e^{\zeta}[K_0(\zeta) + K_1(\zeta)]\,d\zeta \quad \text{when } \zeta > 0 \quad (30b)$$

and using Eqs. (26a), (26b), (29a), (29b) they become

$$Q^* = -\frac{1}{\pi}\left[2\,|\zeta|\,e^{-|\zeta|}[K_0(|\zeta|) - K_1(|\zeta|)] + e^{-|\zeta|}K_0(|\zeta|)\right] \quad \text{when } \zeta < 0 \quad (31a)$$

$$Q^* = \frac{1}{\pi}\left[2\zeta e^{\zeta}[K_0(\zeta) + K_1(\zeta)] - e^{\zeta}K_0(\zeta)\right] \quad \text{when } \zeta > 0 \quad (31b)$$

The value of dimensionless wall heat flux within a region between any two x values, e.g., between ζ_1 and ζ_2, is the difference between two corresponding Q^* values designated as $Q^*_{1,2}$. These functions have the unique numerical behaviors discussed in the next section.

5. Results and discussion

An examination of Eqs. (19a) and (19b) shows that there is a significant amount of energy transport by conduction to the fluid before arrival to the heated region. This causes the temperature of the fluid to rise before passing through the $x = 0$ plane. The temperature when $x = 0$ is obtainable from Eq. (19a) or Eq. (19b). The limiting value of the second term within the square brackets in Eq. (19a), as $x \to 0$, is $\pi/2$. Therefore, when $x = 0$, the integration of Eq. (19a) or Eq. (19b) yields the function $\theta(0, y)$ as

$$\theta(0,y) = \frac{1}{2} - \frac{\omega y}{2}[K_0(\omega y)L_{-1}(\omega y) + K_1(\omega y)L_{-0}(\omega y)] \quad (32a)$$

where $L_{-1}(\omega y)$ and $L_0(\omega y)$ are the modified Struve functions defined by Eq. (12.2.1) in [18] as

$$L_v(\omega y) = \left(\frac{\omega y}{2}\right)^{v+1}\sum_{m=0}^{\infty}\frac{(\omega y/2)^{2m}}{\Gamma(m+3/2)\Gamma(m+v+3/2)} \quad (32b)$$

Fig. 2 represents the behavior of the function $\theta(0, y)$ for different values of ω. Note that, as $\omega \to 0$, the function $\theta(0, y)$ approaches the 1/2 as obtainable from Eq. (5a) when $\phi = \pi/2$. However, when $\omega > 0$, the function $\theta(0, y)$ asymptotically approaches zero and more rapidly as ω becomes very large. This indicates that the effect of the axial conduction becomes small when ω is much larger than those appearing in Fig. 2.

Another interesting feature is observation of energy gained by the fluid before arrival to $x = 0$ plane. By standard definition, the total grained energy E is

$$E = \int_0^{\infty}\rho c_p U[T(0,y) - T_i]W\,d\hat{y} \quad (33a)$$

that can be written as

$$\frac{E/W}{k\{T_w - T_i\}} = 2\int_0^{\infty}\left(\frac{\rho c_p U L_c}{2k}\right)\frac{[T(0,y) - T_i]}{\{T_w - T_i\}}\,d\left(\frac{\hat{y}}{L_x}\right) = 2\omega\int_0^{\infty}\theta(0,y)\,dy \quad (33b)$$

The integration of Eq. (15a) or Eq. (15b), when $x = 0$, would provide the value of the integral in the above equation, that is

$$\begin{aligned}\int_0^{\infty}\theta(0,y)\,dy &= \frac{\omega}{\pi}\int_{y=0}^{+\infty}\left(\int_{\lambda=0}^{+\infty}\frac{e^{-y\sqrt{\lambda^2+\omega^2}}}{\lambda^2+\omega^2}\,d\lambda\right)dy \\ &= \frac{1}{\pi}\int_{\lambda=0}^{+\infty}\left(\int_{y=0}^{+\infty}e^{-y\sqrt{\lambda^2+\omega^2}}\,dy\right)\frac{\omega}{\lambda^2+\omega^2}\,d\lambda \\ &= \frac{1}{\pi}\int_{\lambda=0}^{+\infty}\frac{\omega}{(\lambda^2+\omega^2)^{3/2}}\,d\lambda \\ &= \frac{\lambda}{\pi\omega\sqrt{\lambda^2+\omega^2}}\Bigg|_{\lambda=0}^{\infty} = \frac{1}{\pi\omega}\end{aligned} \quad (34)$$

After substitution of this integral in Eq. (33b), the energy gained by the fluid before its arrival to $x = 0$ plane is

$$\frac{E/W}{k\{T_w - T_i\}} = \frac{2}{\pi} \quad (35)$$

which is a constant, independent of velocity. This is consistent with the temperature data in Fig. 2 that show the local temperature decreases as velocity or ω increases.

The computed numerical data are acquired from Eqs. (23a) and (23b) for the study of the Stanton number variations. The solid lines in Fig. 3 show the values of $St = h/(\rho c_p U)$ from Eqs. (23a) and (23b) representing the

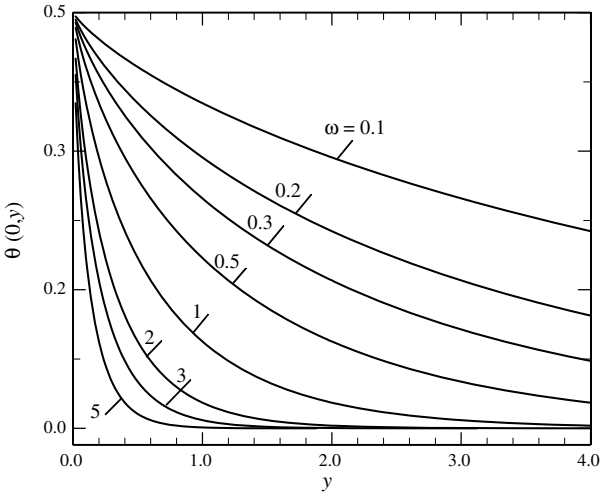

Fig. 2. Dimensionless temperature $\theta(0,y)$ at $x=0$ for different ω values.

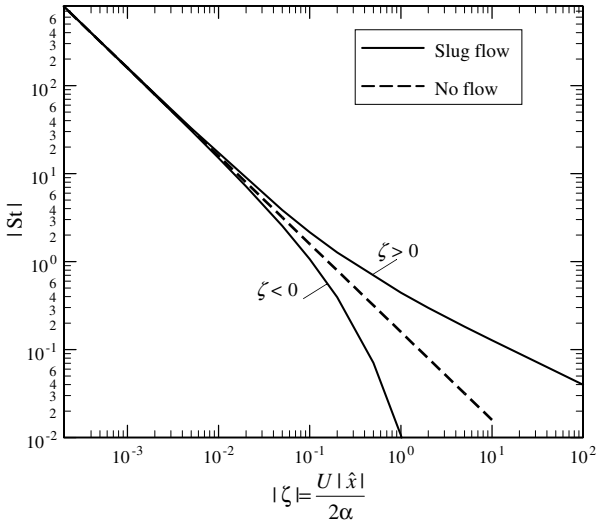

Fig. 3. The Stanton number St as a function of $|\zeta| = U|\hat{x}|/(2\alpha)$.

Table 1
Selected values of St, Q^*, and Nu_x for heat transfer in slug flow over an infinite plate, when $x<0$

$-Pe_x/2$	$-St$	Q^*, Eq. (30a)	Nu_x	$-1/(\pi Pe_x)$
10	6.28×10^{-12}	-5.87×10^{-12}	1.25×10^{-10}	0.015916
5	3.79×10^{-07}	-3.35×10^{-07}	3.78×10^{-06}	0.031831
2	0.0006	−0.0004	0.00224	0.0796
1	0.0106	−0.0069	0.02118	0.1592
0.5	0.0707	−0.0371	0.07066	0.3183
0.2	0.3939	−0.1416	0.15758	0.7958
0.1	1.0695	−0.2712	0.21391	1.5916
0.05	2.5427	−0.4344	0.25427	3.1831
0.02	7.1647	−0.6837	0.28659	7.9578
0.01	15.009	−0.8875	0.30018	15.916
0.005	30.813	−1.0986	0.30812	31.831
0.002	78.412	−1.3838	0.31365	79.578
0.001	157.88	−1.602	0.31576	159.16
0.0005	316.92	−1.8213	0.31692	318.31
0.0002	794.24	−2.1121	0.3177	795.78
0.0001	1589.9	−2.3324	0.31798	1591.6
0.00005	3181.4	−2.5529	0.31814	3183.1
0.00002	7955.9	−2.8444	0.31823	7957.8
0.00001	15914	−3.065	0.31827	15916
0.000001	159153	−3.7979	0.31831	159155

variation of St when $x<0$ and when $x>0$. According to data in Table 1, the function St is negative when $x<0$ while the graph describes the changes in its absolute values; for this case, the St values rapidly approach zero. When $x>0$, the Stanton number has a higher value. The dash line in Fig. 3 shows the limiting values of these data obtained from Eq. (16), under the no flow condition. It is remarkable that, at small x values, these two sets of data from Eqs. (23a) and (23b) approach the dash line for $St=1/(\pi Pe_x)$ when $|\zeta|<0.01$. This limiting value for the no flow condition implies that, at small x values, the data for all velocities behave similarly. In other words, for sufficiently small values of x, the heat transfer is dominated by heat conduction; the flow velocity has negligible effect there. A similar behavior is detectable by examination of the Nusselt number. The Nusselt number $Nu_x=h\hat{x}/k$ is a product of the Stanton number and the Peclet number and it is obtainable from the relation

$$Nu_x = St\times Pe_x = \frac{h}{\rho c_p U}\times\frac{U\hat{x}}{\alpha}=\frac{h\hat{x}}{k} \tag{36}$$

The data plotted in Fig. 4 show the values of the Nusselt number $Nu_x=h\hat{x}/k$ as a function of $|\zeta|=|Pe_x|/2$, for both positive and negative values of ζ. Both sets of data asymptotically approach the value of $1/\pi$, which is obtainable under no flow condition. This observation is consistent with other observations that, in the neighborhood of the thermal entrance location, the heat transfer coefficient becomes nearly independent of the velocity and it varies as $1/x$, when $|Pe_x|$ is between 0 and 0.01 for both positive and negative values of x.

One unique and a major issue is the functional behavior of Q^*. According to Eq. (31a), $Q^*\to 0$ as $\zeta\to-\infty$ and,

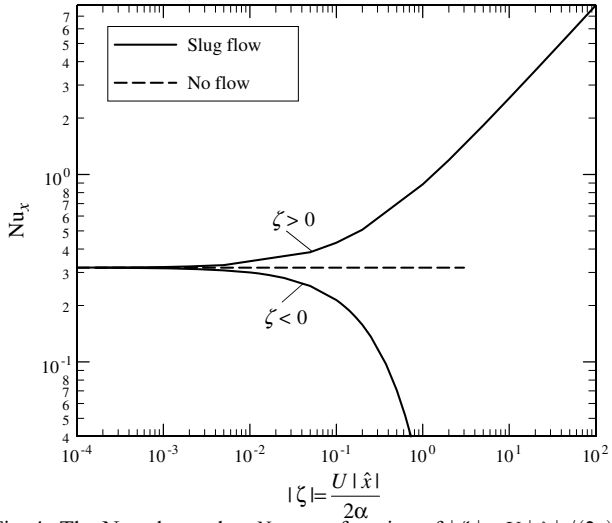

Fig. 4. The Nusselt number Nu_x as a function of $|\zeta| = U|\hat{x}|/(2\alpha)$.

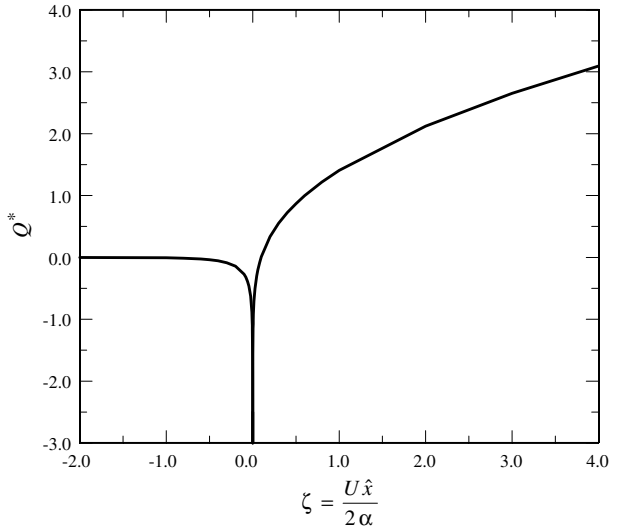

Fig. 5. Total wall heat flux as a function of $\zeta = U\hat{x}/(2\alpha)$ from Eqs. (30a) and (30b).

therefore, Q^* stands for $Q^*(\zeta) = Q^*_{-\infty,\zeta}$ when $\zeta < 0$. This indicates that the Q^* entries in Table 1 are the dimensionless total wall heat flux between $\zeta = -\infty$ and $\zeta < 0$ and Fig. 5 shows this trend when $\zeta < 0$. Also, integration from $\zeta = -\infty$ to any x on the positive sides is possible. Such integration leads to the quantity Q^* from Eq. (31b) for the positive ζ values. It is noted that, as $\zeta \to 0$ on the negative side, the total wall heat flux becomes infinite. Furthermore, the function Q^* in Eq. (31b) goes to $-\infty$ as $\zeta \to 0$ and it goes to $+\infty$ as $\zeta \to \infty$.

Fig. 6 shows the values of $Q^*_{-\infty,\zeta}$ depicted as $|\,Q^*_{-\infty,\zeta}\,|$ for $\zeta < 0$ and the values of $Q^*_{\varepsilon,\zeta} = Q^*(\zeta) - Q^*(\varepsilon)$ when $\varepsilon = 10^{-6}$ for $\zeta > 0$, using the data in Table 2. Therefore, the function $Q^*_{\varepsilon,\zeta}$ represents the total dimensionless heat flux leaving the plate between $\zeta = \varepsilon$ and a $\zeta > 0$ value. The selected value of $\varepsilon = 10^{-6}$ is sufficiently small so that below which the continuum state of materials may not be valid. Using this lower limit for $\zeta = \varepsilon$, the corresponding x value is $\hat{x} = (2\alpha/U) \times 10^{-6}$ m. For a typical liquid metal thermal diffusivity with $\alpha = 10^{-5}$ m^2/s, this distance is $\hat{x} = 0.02/U$ nm. In general, the continuum condition is not valid for a range of $-\varepsilon < \zeta < \varepsilon$ when ε is of the order of molecular dimension. As an illustration, typical atomic radii of materials vary between 0.071 nm for Nitrogen atoms and 0.265 nm for Cesium atoms, as given in [20]. For $\varepsilon = 10^{-6}$, $\alpha = 10^{-5}$ m^2/s, and a velocity of $U = 2$ cm/s, the corresponding $\hat{x}$ value is 1 nm, of the order of atomic dimension. A similar situation emerges when a fluid flows through a porous passage. As $\hat{x}$ reduces and become of the order of pore size, the local heat transfer coefficient cannot exceed that within the pores. The value of interstitial heat transfer, as given in Wakao and Kaguei [21], for stationary fluid in a packed bed of spherical particles is $hd/k = 2$, where d is the diameter of the spheres. Using pure conduction through different-shaped pores, Minkowycz et al. [22] introduced the values of hr_h/k that change between 1.09 and 1.45, where r_h is the hydraulic radius of the pores as defined in [22]. In general, it is possible to use the data in Tables 1 and 2 for the determination wall heat flux between any two ζ_1 and ζ_2 values from the equation

$$Q^*_{\zeta_1,\zeta_2} = Q^*_{\varepsilon,\zeta_2} - Q^*_{\varepsilon,\zeta_1} = Q^*(\zeta_2) - Q^*(\zeta_1) \tag{37}$$

if ζ_1 and ζ_1 are within a range that the assumption of continuum condition is valid. However, if the parameter $\zeta_1 < 0$ and $\zeta_2 > 0$, there would be a jump in the heat flux at $\zeta = 0$ due to the mathematical formulation. It is noted that this jump in the total wall heat flux appears within a range that

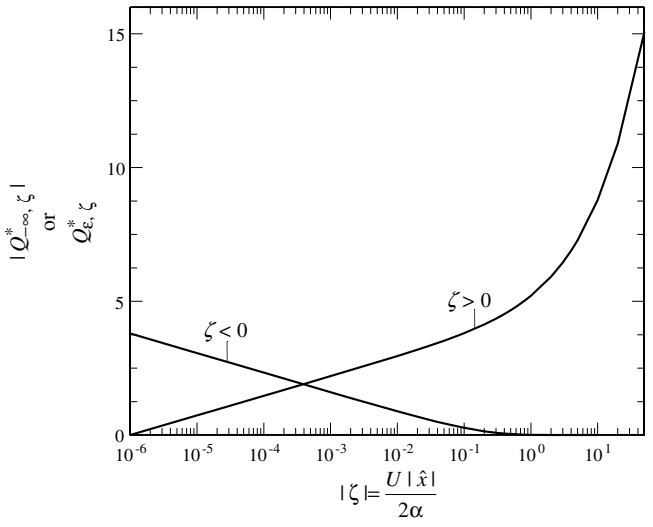

Fig. 6. Total wall heat flux as a function of $|\zeta| = U|\hat{x}|/(2\alpha)$ when $\varepsilon = 10^{-6}$.

Table 2
Selected values of St, Q^*, and Nu_x for heat transfer in slug flow over an infinite plate, when $x > 0$

$Pe_x/2$	St	Q^*, Eq. (30b)	Nu_x	$1/(\pi Pe_x)$
100	0.0399	15.938	7.9888	0.0016
50	0.0566	11.256	5.6559	0.0032
20	0.0898	7.0920	3.5903	0.0080
10	0.1277	4.9836	2.5541	0.0159
5	0.1827	3.4801	1.8272	0.0318
2	0.2984	2.1195	1.1937	0.0796
1	0.4425	1.4059	0.8851	0.1592
0.5	0.6772	0.8693	0.6772	0.3183
0.2	1.2691	0.3339	0.5077	0.7958
0.1	2.1601	0.0102	0.4320	1.5916
0.05	3.8523	−0.2717	0.3852	3.1831
0.02	8.7653	−0.6070	0.3506	7.9578
0.01	16.830	−0.8447	0.3366	15.916
0.005	32.854	−1.0750	0.3285	31.831
0.002	80.745	−1.3731	0.3230	79.578
0.001	160.43	−1.5962	0.3209	159.16
0.0005	319.70	−1.8182	0.3197	318.31
0.0002	797.31	−2.1107	0.3189	795.78
0.0001	1593.2	−2.3317	0.3186	1591.6
0.00005	3184.9	−2.5525	0.3185	3183.1
0.00002	7959.7	−2.8442	0.3184	7957.8
0.00001	15918	−3.0649	0.3184	15916
0.000001	159157	−3.7979	0.3183	159154

the continuum condition does not apply. This leads to a transition region to be followed by a non-continuum region in which h has a nearly constant mean value, although it locally varies due to molecular or other interactions. Therefore, a properly selected ε depends on the specific application. Ignoring the transition region and assuming $h \cong \bar{h}$ to be a constant within the non-continuum region, Eq. (24a) provides an estimation for the value of $Q^*_{0,\varepsilon} = \bar{h}\hat{x}/k$ for $\hat{x}_1 = 0$ and $\hat{x}_2 = \hat{x} = 2\alpha\varepsilon/U$. Since $\zeta = \varepsilon$ is very small, Eq. (24) yields $\bar{h}\hat{x}/k \cong h(\zeta)\hat{x}/k \cong 1/\pi$, as can be seen from the data plotted in Fig. 4. This makes the total wall heat flux within a region between $\zeta = 0$ and $\zeta > \varepsilon$ to become

$$Q^*_{0,\zeta} = Q^*_{0,\varepsilon} + Q^*_{\varepsilon,\zeta} \cong \frac{1}{\pi} + Q^*(\zeta) - Q^*(\varepsilon) \tag{38}$$

and $\varepsilon = U\hat{x}/(2\alpha)$ is located where the continuum condition begins, within $\zeta \geqslant \varepsilon$ region. Also, since ε is very small, this equation is valid when $\zeta < 0$ although, by definition, $Q^*_{0,\zeta} = -Q^*_{\zeta,0}$.

6. Conclusion

It is shown that the heat transfer rate at sufficiently small values of x is independent of the magnitude of the velocity, represented as the Peclet number. Indeed, even the no flow and slug flow conditions provide reasonable limiting values near the thermal entrance location. Additionally, this limiting concept is valuable for determination of wall heat flux at the entrance regions of parallel plate ducts, circular pipes, and those with two-dimensional cross sections such as rectangular and triangular ducts. There are various passages in engineering applications within which the axial conduction should not be ignored.

Furthermore, these limiting values show that the value of total wall heat flux between 0 and a very small $x = \varepsilon$ may not be deterministic. This is expected since the value of wall heat flux at $x = 0$ is infinite due to the step change in temperature. However, this is not a serious issue because ε can be set to have an extremely small value as the lower limit for the continuum condition.

References

[1] H.S. Carslaw, J.C. Jaeger, Conduction of Heat in Solids, second ed., Oxford University Press, New York, 1959.
[2] J.V. Beck, K.D. Cole, A. Haji-Sheikh, B. Litkouhi, Heat Conduction Using Green's Functions, Hemisphere Publ. Corp., Washington, DC, 1992.
[3] Ş. Bilir, Laminar flow heat transfer in pipes including two-dimensional wall and fluid axial conduction, Int. J. Heat Mass Transfer 38 (9) (1995) 1619–1625.
[4] Ş. Bilir, Transient conjugated heat transfer in pipes involving two-dimensional wall and axial fluid conduction, Int. J. Heat Mass Transfer 45 (8) (2002) 1781–1788.
[5] I. Tiselj, G. Hetsroni, B. Mavko, A. Mosyak, E. Pogrebnyak, Z. Segal, Effect of axial conduction on the heat transfer in microchannels, Int. J. Heat Mass Transfer 47 (12–13) (2004) 2551–2565.
[6] B. Weigand, D. Lauffer, The extended Graetz problem with piecewise constant wall temperature for pipe and channel flows, Int. J. Heat Mass Transfer 47 (24) (2004) 5303–5312.
[7] M.L. Michelsen, J. Villadsen, The Graetz problem with axial heat conduction, Int. J. Heat Mass Transfer 17 (11) (1974) 1391–1402.
[8] J. Lahjomri, A. Oubarra, Analytical solution of the Graetz problem with axial conduction, ASME J. Heat Transfer 121 (4) (1999) 1078–1083.
[9] D.A. Nield, A.V. Kuznetsov, M. Xiong, Thermally developing forced convection in a porous medium: parallel plate channel with walls at uniform temperature, with axial conduction and viscous dissipation effects, Int. J. Heat Mass Transfer 46 (4) (2003) 643–651.
[10] D.A. Nield, A.V. Kuznetsov, M. Xiong, Thermally developing forced convection in a porous medium: circular ducts with walls at constant temperature, with longitudinal conduction and viscous dissipation effects, Transport Porous Med. 53 (3) (2003) 331–345.
[11] P.-X. Jiang, M.-H. Fan, G.-S. Si, Z. Ren, Thermal-hydraulic performance of small scale micro-channel and porous-media heat-exchangers, Int. J. Heat Mass Transfer 44 (5) (2001) 1039–1051.
[12] J.L. Lage, A.K. Weinert, D.C. Price, R.M. Weber, Numerical study of low permeability micorporous heat sink for coiling phased-array radar systems, Int. J. Heat Mass Transfer 39 (1996) 3622–3647.
[13] J.L. Lage, A. Narasimhan, Porous media enhanced forced convection fundamentals and applications, in: K. Vafai (Ed.), Handbook of Porous Media, Marcel Dekker, New York, 2000, pp. 357–394.
[14] D.A. Nield, A. Bejan, Convection in Porous Media, third ed., Springer-Verlag, New York, 2006.
[15] N. Dukhan, R. Picon-Feliciano, Á.R. Álvarez-Hernandez, Heat transfer analysis in metal foams with low-conductivity fluids, ASME J. Heat Transfer 128 (8) (2006) 784–792.
[16] W.J. Minkowycz, A. Haji-Sheikh, Heat transfer in parallel plates and circular porous passages with axial conduction, Int. J. Heat Mass Transfer 49 (13–14) (2006) 2381–2390.
[17] A. Erdelyi, W. Magnus, F. Oberhettinger, F.G. Tricomi, Tables of Integral Transforms, vol. 1, McGraw-Hill, New York, 1954.
[18] I.S. Gradshteyn, I.M. Ryzhik, in: Alan Jeffrey (Ed.), Table of Integrals, Series, and Products, fifth ed., Academic Press, Inc., 1994.
[19] M. Abramowitz, I.A. Stegun, Handbook of Mathematical Functions, National Bureau of Standards Applied Mathematics Series 55, 1965.
[20] J.F. Shackelford, Introduction to Materials Science for Engineers, fourth ed., Prentice Hall, Inc., New Jersey, 1996.
[21] N. Wakao, S. Kaguei, Heat and Mass Transfer in Packed Beds, Gordon and Breach Science Publication, 1982.
[22] W.J. Minkowycz, A. Haji-Sheikh, K. Vafai, On departure from local thermal equilibrium in porous media due to a rapidly changing heat source. The sparrow number, Int. J. Heat Mass Transfer 42 (18) (1999) 3373–3385.